JOURNAL OF GEOPHYSICAL RESEARCH: ATMOSPHERES, VOL. 118, 9534–9551, doi:10.1002/jgrd.50694, 2013

Observed frequency and intensity of tropical precipitation from instantaneous estimates

Michela Biasutti[1] and Sandra E. Yuter[2]

Received 4 March 2013; revised 30 July 2013; accepted 30 July 2013; published 5 September 2013.

[1] Negative societal impacts can result from intense individual downpours, the accumulation of rainfall over a day or more, or a combination of these. Accumulation is reasonably well captured by daily reporting rain gauges, but rainfall intensity is not. Ten years of data from the Tropical Rainfall Measuring Mission (TRMM) Precipitation Radar (PR) are used to describe the spatial and seasonal distributions of instantaneous rainfall intensity with an emphasis on how these differ from the distributions of mean daily accumulation. Over tropical land, the rainy season, when rainfall is most frequent, does not coincide with the highest mean intensity. Rather, intensity peaks just before the rainy season. This offset is most obvious in the pre-onset and post-onset months in monsoon regions and it is also evident in equatorial regions without a well-defined dry and rainy season. Most seasonal variations in rainfall intensity can be explained as parallel variations in the occurrence of convective, relative to stratiform, precipitation. However, regional differences in rainfall intensity are related to differences in the intensity of convection itself. Compared with seasonal changes in intensity over land, variations in convective precipitation fraction over tropical oceans are trivial, and the modest seasonal changes in the intensity of rainfall parallel those of frequency. These findings suggest that studies of precipitation extremes under global warming should (1) explicitly tackle the question of changes in the intensity of rainfall separately from changes in daily rainfall accumulation and (2) consider the different qualities of extreme precipitation events over ocean and over land.

Citation: Biasutti, M., and S. E. Yuter (2013), Observed frequency and intensity of tropical precipitation from instantaneous estimates, *J. Geophys. Res. Atmos.*, *118*, 9534–9551, doi:10.1002/jgrd.50694.

1. Introduction

[2] The impact of a rainfall event depends on how it unfolds as much as on the final rainfall tally. For example, 1.5 inches of rainfall in 24 h in New York City may not have a significant negative effect. However, if the same rain falls within an hour in an intense downpour, it can cripple the subway system (http://cityroom.blogs.nytimes.com/2007/08/08/why-do-the-subways-flood/). Thus, knowledge of the statistics of rainfall and rainfall extremes at a wide range of timescales is highly desirable. Climate monitoring of global rainfall typically uses daily rain gauge accumulation reports, but these observations have key limitations. First, the vast majority of gauges are on land (with the exception of a small number of buoys, e.g., *McPhaden et al.* [1998]). Second, daily rain gauge reports provide only information on accumulation, not rainfall intensity or duration. As a consequence, most of the research on climate change and rainfall extremes is limited to the daily timescale—even though the expectation of more extreme precipitation under global warming comes from the link between atmospheric humidity and rainfall at the scale of convection [*Allen and Ingram*, 2002; *Trenberth et al.*, 2003]. For example, *Alexander et al.* [2006], *Tebaldi et al.* [2006], and *O'Gorman and Schneider* [2009] have looked at observed trends and projections for daily accumulation. Modeling studies that are relevant for trends in hourly precipitation rates are idealized [e.g., *Muller et al.*, 2011] or focus on trends in the occurrence and severity of tropical cyclones and extra-tropical severe storms [e.g., *Vecchi and Soden*, 2007; *Knutson et al.*, 2010; *Trapp et al.*, 2007]. Observational studies of hourly precipitation trends are limited to a few stations [*Lenderink and Van Meijgaard*, 2008; *Lenderink and van Meijgaard*, 2010; *Shaw et al.*, 2011; *Lenderink et al.*, 2011].

[3] For their part, meteorologists have traditionally looked at rainfall extremes in terms of individual intense storms. While isolated storms can produce heavy rainfall on scales of minutes, the majority of tropical rainfall is associated with mesoscale convective systems (MCS) or mesoscale convective complexes (MCC), and research

[1]Lamont-Doherty Earth Observatory, Columbia University, Palisades, New York, USA.
[2]Department of Marine, Earth, and Atmospheric Sciences, North Carolina State University, Raleigh, North Carolina, USA.

Corresponding author: M. Biasutti, Lamont-Doherty Earth Observatory, Columbia University, 61 Route 9W, Palisades, NY 10964-8000, USA. (biasutti@ldeo.columbia.edu)

2169-897X/13/10.1002/jgrd.50694

has focused on explaining the conditions that make these storms possible. Moisture, lift, and instability must all be present for convective-type precipitation to occur [*Schultz and Schumacher*, 1999]. Forecasters usually look first for convective available potential energy (CAPE; the integrated positive buoyancy of an air parcel at the surface, or in the boundary layer, from the level of free convection to the equilibrium level) to determine if moisture and instability are present. Next, they look at convective inhibition (CIN; the work needed to lift the parcel to its level of free convection) and sources of lift to overcome CIN to determine if storms will develop. Finally, they look at vertical wind shear for information on how the convective storms will be organized [*Markowski and Richardson*, 2010]. *Laing and Fritsch* [2000] characterized the mean genesis environments for MCC as having locally strong values of both CAPE and low-level vertical wind shear. Values of CAPE and shear from soundings proximate to intense events can be combined to discriminate environments prone to severe weather [e.g., *Brooks et al.*, 2003]. However, because these environments are transient and CAPE is rapidly consumed by convective activity, simple temporal averages of CAPE and shear are not well correlated with the occurrence of mesoscale convective systems.

[4] A climatology of storm characteristics in the entire tropical band has been made possible with the collection of more than a decade of observations from the Tropical Rainfall Measuring Mission (TRMM). These data can provide a broader view on the conditions for intense precipitation events, clarify the relationship between the intensity of rainfall events and rainfall accumulation, and narrow the gap between the views of climatologists and meteorologists. For example, *Zipser et al.* [2006] used several measurements of cloud and hydrometeor characteristics to identify the geographical distribution of intense storms and weaker precipitation systems. In their conclusions, they noted a discrepancy between intense storms and heavy seasonal rainfall: "The strongest convective storms are often found in semiarid regions, while the heavy rains of the oceanic ITCZ, western Amazonia, and much of southeast Asia and Indonesia have relatively few intense storms. In parts of the Indian subcontinent, the most intense storms occur in the premonsoon months, while the rainiest parts of the monsoon consist of numerous weather systems but few severe storms" [*Zipser et al.*, 2006].

[5] These conclusions are supported by a number of other studies based on TRMM data that focus on selected regions and seasons. For example, *Schumacher and Houze* [2006] noted the lower intensity and higher frequency of rainfall events over the Atlantic compared with West Africa and also noted that the monsoon season is characterized by factors favorable for production of stratiform rain—lower values of upper level shear and higher convective sustainability, i.e., an environment that can support continual formation of new convective cells [*Yuter and Houze*, 1998]. Similarly, *Kodama et al.* [2005] observed stronger convection and lightning activity during the premonsoon season in South America and India than during the monsoon season. More recently, *Romatschke et al.* [2010] noted that deep convective cores are characteristic of the premonsoon season of India, and organized convective systems with large stratiform components are typical of the monsoon season. *Williams et al.* [2002] examined the seasonal evolution of thunderstorm activity in conjunction with environmental variations in CAPE and aerosols to understand if the latter can play a role in modulating lightning. Additionally, they indicated that, under certain conditions present in the western Amazon, the lines between maritime rains and continental showers [*Ramage*, 1971] are blurred. *Liu* [2011] mapped several measures of precipitation feature intensity (including echo top height, maximum height of 30 dBZ contour, and minimum 85 GHz TRMM Microwave Imager polarization-corrected brightness temperatures) and showed that the storms with largest graupel and hail, and thus strongest updrafts, occurred in Equatorial Africa and Argentina.

[6] In *Biasutti et al.* [2011], we used near-surface reflectivity values from the TRMM Precipitation Radar (PR) to create a 10 year (1998–2007) monthly climatology of frequency of rain (*f*; the percentage of satellite snapshots in which rainfall is detected) and of mean conditional intensity (*i*; the mean rainfall calculated over rainy snapshots) at the original radar resolution of 0.05°× 0.05°. This data set portrays the mean characteristics of precipitation events and thus is a variation of the TRMM-derived storm climatology of *Zipser et al.* [2006]. Rainfall frequency, which is dominated by weak and moderate-intensity precipitation systems, is highest over the precipitation centers of the ocean (i.e., those with high monthly rain rates such as the Pacific and Atlantic Intertropical Convergence Zones (ITCZs), the Warm Pool, and the Bay of Bengal). Rainfall reaches similar peak frequencies over land only in the Amazon and over mountain ranges. Conditional intensity, on the other hand, clearly identifies regions with a propensity for very intense storms, such as the Himalayan Indentation [see also *Zipser et al.*, 2006; *Romatschke et al.*, 2010]. However, in general, conditional intensity presents weaker and broader spatial variations than frequency. Intensities are often higher over land than ocean (as shown by multiple previous studies using measurements as different as lightning frequency and cloud top temperatures, e.g., *Zipser et al.* [2006]; *Liu and Zipser* [2009]).

[7] Peak intensity values are found in the subtropical latitudes of both North and South America, in the Congo Basin, and in the Himalayan indentation, while the Amazon has rainfall intensities between typical oceanic and continental values. The annual mean and seasonal mean patterns of frequency and conditional intensity presented in *Biasutti et al.* [2011] are consistent with previous literature on storm characteristics [e.g., *McCollum et al.*, 2000; *Williams et al.*, 2002; *Schumacher and Houze*, 2003; *Romatschke and Houze*, 2010; *Romatschke et al.*, 2010], and the agreement indicates that this data set can be used to investigate spatial and seasonal variations in storm characteristics across the tropics.

[8] In this study, we use the TRMM PR tropic-wide data set to systematically document estimated rainfall frequency, conditional intensity, and the relationship between them. We specifically focus on how the relationship between frequency and intensity changes seasonally and across a variety of rainfall regimes, from oceanic to continental and from humid to semiarid. We combine our gridded data set with the precipitation feature data set of the University of Utah Precipitation Measuring Mission [*Nesbitt et al.*, 2000; *Liu et al.*,

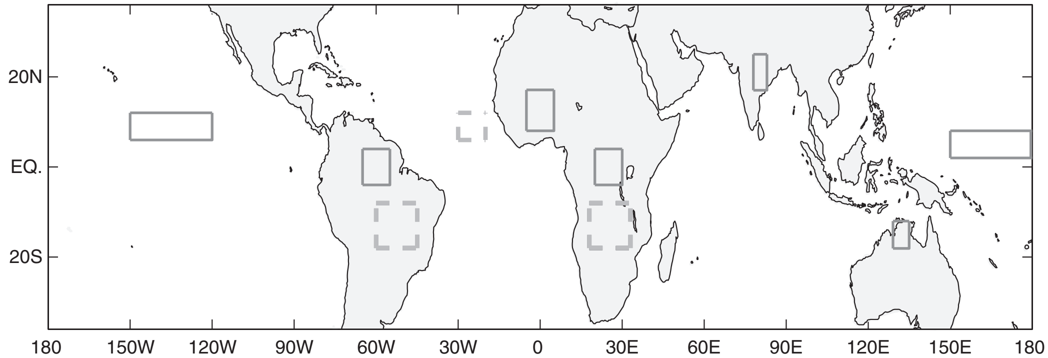

Figure 1. Regions analyzed in this study. Dashed boxes indicate regions that were analyzed but not shown in additional figures.

2008], which is organized by storm, to interpret our results in terms of storm characteristics, namely the prevalence of stratiform or convective rainfall. Finally, we investigate if the kind of data currently available from climate simulations, specifically the daily aggregated values of convective and large-scale (stratiform) rainfall, is sufficient to describe the rainfall events, or if additional model output is needed to compare model simulations and observations at the storm timescale.

[9] This study complements previous work by authors at the University of Utah using their precipitation feature data set (initially developed by *Nesbitt et al.* [2000] and further refined by *Liu et al.* [2008]), including *Toracinta et al*. [2002], *Nesbitt and Zipser* [2003], *Nesbitt et al.* [2004], *Cecil et al.* [2005], *Liu and Zipser* [2005], *Nesbitt et al.* [2006], *Zipser et al.* [2006], and *Liu and Zipser*, [2008, 2009]. The focus of the current paper is on an aspect of global precipitation that was not fully addressed in previous work: the relationship between precipitation frequency and conditional intensity and how this relationship changes geographically and seasonally. We emphasize a comparison of climatological variations in storm intensity obtained from instantaneous rainfall measurements to climatological variations in mean daily accumulation on rainy days, a more common measure of rainfall intensity in climate studies. *Dai* [2001] examined global precipitation frequency using weather reports from the Comprehensive Ocean-Atmosphere Data Set (COADS) and inferred seasonal mean intensity by dividing the *Xie and Arkin* [1997] infrared-based seasonal precipitation estimates by seasonal frequency. In contrast, this study uses TRMM PR data for both frequency of precipitation and conditional rain rate (intensity), the latter of which is a better proxy for rain rates within individual storms than seasonal mean intensity.

[10] Section 2 introduces the data sets used in this study and defines the relationship between our snapshot-based definition of frequency and intensity to the comparable variables obtained from daily aggregated data, namely the frequency of rainy days and the mean daily accumulated rainfall on rainy days. Section 3 describes our methodology using the central India region as an example. For this region, we analyze both instantaneous and daily frequency and intensity, and we describe how instantaneous conditional intensity peaks before frequency during the premonsoon seasons. In addition, we explain this result in terms of predominantly convective rainfall before the monsoon onset. Section 4 generalizes our findings for most of the tropical land masses, both those that experience a dry season and those that are quite rainy throughout the year. We also highlight the contrast between land and oceanic regions. The regions focused on in this study are shown in Figure 1. Section 5 discusses if daily aggregated data of the kind climate models customarily archive is sufficient to characterize mean storm intensity. Section 6 offers our summary and conclusions.

2. Data and Methods

2.1. Data Sets

[11] The TRMM PR [*Kummerow et al.*, 2000] provides a unique opportunity to observe the climatology of rainfall in great detail with the same instrument over tropical land and ocean locations. Coverage extends to about 36°N/S, and the precessing orbit of the TRMM satellite permits nearly uniform sampling across the diurnal cycle [*Negri et al.*, 2002; *Hirose and Nakamura*, 2005]. We use a 1998–2007 monthly climatology [*Biasutti et al.*, 2011] obtained by (1) binning the TRMM PR Version 6 data from each individual swath onto a regular grid with spacing of 0.05° in both longitude and latitude (about a 5 km grid) and (2) averaging the gridded data over the entire record to produce monthly climatologies. A minimum of about 1700 observations per grid point (up to a maximum of over 8000) are used.

[12] Rainfall frequency at any location is defined as the number of observations in which a radar reflectivity Z is detected to be above the threshold of 18 dBZ, normalized by the total number of observations. This sensitivity threshold implies that drizzle events are not captured by the TRMM PR. As a measure of conditional rainfall intensity, we use the mean reflectivity when rain is detected (i.e., the averaging does not include dry states). Note that while the TRMM PR data also provide rainfall rates, there is some uncertainty in the rain/reflectivity (R/Z) conversion [see, for example, *Shige et al.*, 2006]. To bypass this issue, we conduct our analysis using mostly the attenuation-corrected reflectivity. However, rainfall values are used to show that our results are robust to the choice of intensity measure and as an intermediate step in our comparison with daily data. For this analysis, as with the station data described below, a rain event is one with instantaneous rain rates >0.4 mm h^{-1}. When using

reflectivity, averaging is performed on the reflectivity Z itself ($mm^6\ m^{-3}$), and the conversion to dBZ is applied as the last step of the calculation. The log-normal distributions of both rainfall in mm h^{-1} and reflectivity in $mm^6\ m^{-3}$ yield a near-linear relationship between dB of rainfall and reflectivity in dBZ and allows us to loosely interpret mean reflectivity as mean rainfall intensity. We will refer to the conditional reflectivity as intensity.

[13] Frequency and intensity (f and i) from the TRMM PR data are compared to their daily counterparts obtained from TRMM 3B42 Version 6 [*Huffman et al.*, 2007]: the number of rainy days with $\geq$1 mm of accumulation (R1) and the simple daily intensity index (SDII), which is the mean accumulation on rainy days. TRMM 3B42 data are obtained by merging information from the TRMM instruments with infrared and visible sensors on geostationary satellites. The TRMM 3B42 product is gridded at 0.25° resolution. In section 3, we contrast results from TRMM 3B42 with the gauge-based gridded 1° × 1° rainfall data from the Indian Meteorological Department (http://www.imd.gov.in/doc/nccraindata.pdf).

[14] We examine the impacts of data aggregation at different temporal scales in section 2.2 using 1 min optical rain gauge data from the U.S. Department of Energy Atmospheric Radiation Measurement (ARM) Climate Research Facility site in Darwin, Australia. Rainfall time series taken from other ARM sites paint the same picture (not shown). Although there are differences between the instantaneous rainfall estimates obtained from different instruments, the description of the role of temporal aggregation on frequency and intensity time series is independent of the instrumentation as long as the instrument is appropriate for high-frequency sampling.

[15] We focus on a subset of parameters from the *Liu et al.* [2008] precipitation feature database based on TRMM Version 6 products. Individual precipitation feature characteristics are based on orbit overpass data (Level 2). We examine the following variables of each precipitation feature: (1) number of pixels with stratiform rain, (2) number of pixels with convective rainfall, (3) stratiform volumetric rain (km^2 mm h^{-1}), and (4) convective volumetric rain (km^2 mm h^{-1}). The separation of stratiform and convective elements follows *Awaka et al.* [1997] and subsequent refinements [*Liu et al.*, 2008]. The number of pixels multiplied by 25 km^2 is the area covered by the precipitation feature. We also use monthly data (Level 3) from the same precipitation feature database, specifically monthly total convective and stratiform rainfall. The means of the monthly ratios of convective to stratiform rainfall from the University of Utah Level 3 data are compared to those calculated from ERA-Interim estimates of daily convective and large-scale rainfall in section 5. *Dee et al.* [2011] documented the use of observations in producing the ERA-Interim reanalysis and assessed the remaining biases. Annual mean rainfall rates from the Global Precipitation Climatology Project (GPCP, Version 2.1) [*Huffman et al.*, 1997] are used to provide context for and comparison to our rainfall frequency maps.

[16] To test statistical significance of the differences in mean intensities between pre-onset and monsoon or rainy seasons (sections 3 and 4), we use a Monte Carlo analysis in which data points for the two seasons were randomly reassigned to group A or B (a thousand times). The difference in mean intensity (as a function of frequency) between the two seasons was then compared to the 95th (97.5th) percentile in the difference between A and B groups.

2.2. The Effect of Temporal Aggregation on Frequency and Intensity Time Series

[17] Figure 2 shows the annual mean frequency and intensity of rainfall events (f and i) as estimated from the snapshot data of the TRMM PR and the frequency and intensity of rainy days (R1 and SDII) estimated from TRMM 3B42. The annual mean rain rates estimated from GPCP are superimposed. As noted in more detail in *Biasutti et al.* [2011], the intensity i is noisier than frequency f. The geographic variations in i are broad in scale, while f shows sharper spatial gradients. The two patterns have in common the broad distinction between the rainy regions over the continents and the equatorial oceans, on one hand, and the dry subtropics on the other—but there is little similarity in the details. Most variations in annual mean rain rates are captured by variations in f. Similarly, the R1 field is more closely related to overall rain rates than the SDII field (Figures 2c, 2d), yet we see that the distinctions in patterns between the two fields has faded compared with the snapshot-based fields. For example, the maximum rainfall rates in the ITCZs, the Southern Pacific Convergence Zone (SPCZ), and the southern Indian Ocean are visible in the SDII field, and the maximum rainfall along the coast of Myanmar is ascribed to a maximum in SDII and not in R1. The opposite is true for TRMM PR data where higher frequency of rain events is clearly linked to the large rain rates with intensity gradients playing a very minor role. Another clear example of the difference is the Congo Basin. Although this is a region with explosive storms and some of the highest i values in the tropical band [*Zipser et al.*, 2006], it appears in the SDII map as a region of modest daily intensity.

[18] We can ensure that the observed difference between TRMM products is indeed a consequence of the temporal aggregation, rather than just the spatial aggregation or the method of precipitation estimation in the two retrievals, by comparing f and i with R1 and SDII for gauge measurements. As an example, we present measurements from Darwin, Australia, over the course of one rainy season (2010–2011). Figure 3 shows the seasonal evolution of 10 day (dekad) averages of rain frequency and intensity defined from data at increasing temporal aggregation. In Figure 3a, we use optical rain gauge data at 1 min resolution. In Figure 3b, we have aggregated rainfall data at hourly resolution and calculate the 10 day average frequency and intensity using the same definition of rainy event (rain rates >0.4 mm h^{-1}) as for minute-by-minute data. In Figure 3c, we plot R1 and SDII. As the temporal aggregation increases, frequency values increase and intensity values decrease. This result is dependent both on the episodic nature of rainfall in Darwin and on the thresholds that define a rain event or a rainy day. Across Figures 3a–3c, the relationship between dekadal mean frequency and intensity of rainfall changes, in consequence to the fact that the two quantities are defined from rainfall measurements aggregated at increasingly longer times. The changing relationship is exemplified by the way in which events that

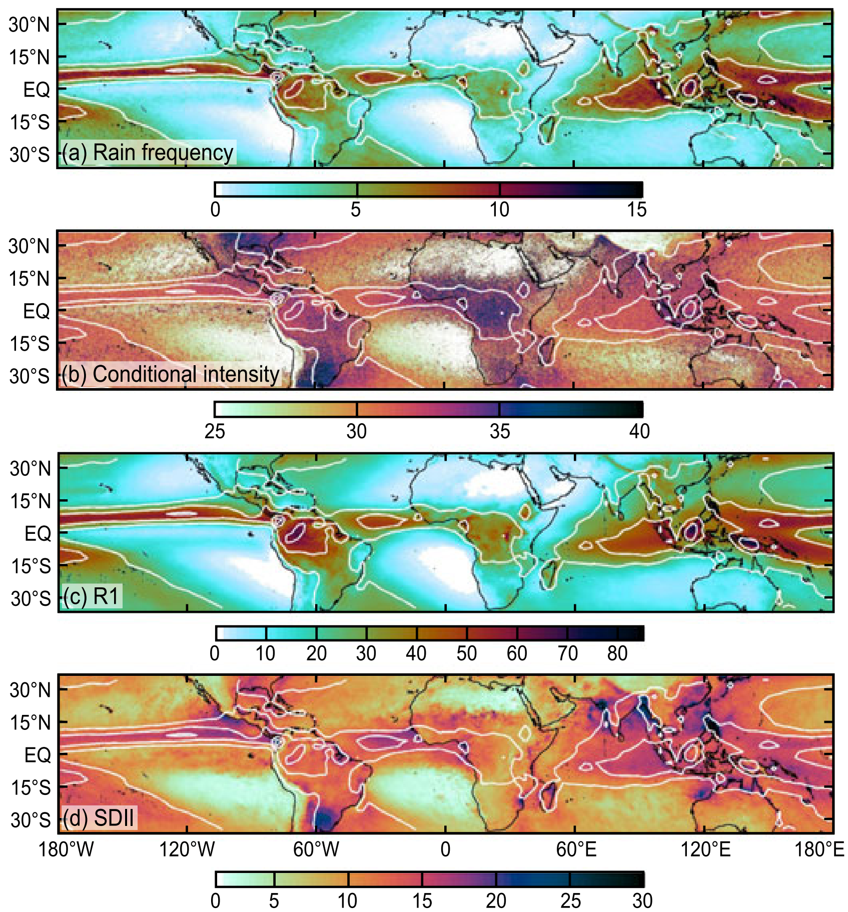

Figure 2. The annual mean frequency and intensity maps from 1998–2007 differ when the fields are defined from instantaneous rainfall values or from diurnally aggregated rainfall values. (a) Frequency (*f*, in percent) and (b) intensity (*i*, in dBZ) from TRMM PR. (c) Percent of rainy days with accumulation >1 mm per day (R1) and (d) simple daily intensity index or mean rainfall accumulation on rainy days (SDII, in mm) from TRMM 3B42. Contours are annual mean rainfall rates from GPCP.

appear as maxima in frequency when the latter is defined from minute-average data (Figure 3a) appear as maxima in daily intensity (Figure 3c). These same events appear as local maxima in both frequency and intensity defined at the intermediate hourly timescales (Figure 3b). One example of this is the large storm to hit Darwin in mid-February 2011, which is visible in the 17th dekadal average. The 1 min averaged data show it was raining 32% of the time during the 10 day period with a conditional rainfall intensity of 11 mm/hr. The R1 value for the same 10 day period indicates that it rained more than 1 mm on 8 out of the 10 days (80%) with SDII (average accumulation) of 4 mm/day. More generally, we note that the correlation between dekadal frequency and intensity increases dramatically going from rainfall data aggregated at the minute to daily timescale. This increase in correlation was also apparent in the map view of Figure 2: The SDII pattern matches the R1 pattern (in the ITCZs, for example) better than the *i* pattern matches the *f* pattern. The spatial correlation is 0.61 for the former (3B42 data) and 0.39 for the latter (PR data).

[19] In the rest of the paper, we take advantage of the high-resolution, snapshot-based TRMM PR data to describe the climatology of rainfall characteristics in a wide range of tropical climates.

3. Seasonal Variations of Rainfall Intensity in India

[20] We have noted above that the snapshot definition of frequency and intensity paints a complex picture of tropical rainfall. On one hand, it highlights the role of rainfall frequency in determining rain rates for a single storm (as seen for Darwin in Figure 3) or in setting the spatial gradients in annual mean rainfall (Figure 2). On the other hand, it highlights the tendency for relatively dry places to have more intense rain than places with more frequent rain, be it land compared to ocean or the Congo compared to the Amazon. In the remainder of this paper, we explore the relationship between rainfall frequency and intensity in the context of the seasonal cycle and show that (1) there is no universal relationship between mean frequency and mean intensity at any given location and (2) mean intensity over most tropical land areas is largest just before the core of the rainy season when frequency becomes largest. We further interpret the latter result in terms of the larger amount of stratiform precipitation relative to convective precipitation in the rainy season. In this section, we focus on a region in central India, which permits us to present our methodology in more detail and to compare our results to an additional data set based on gauge

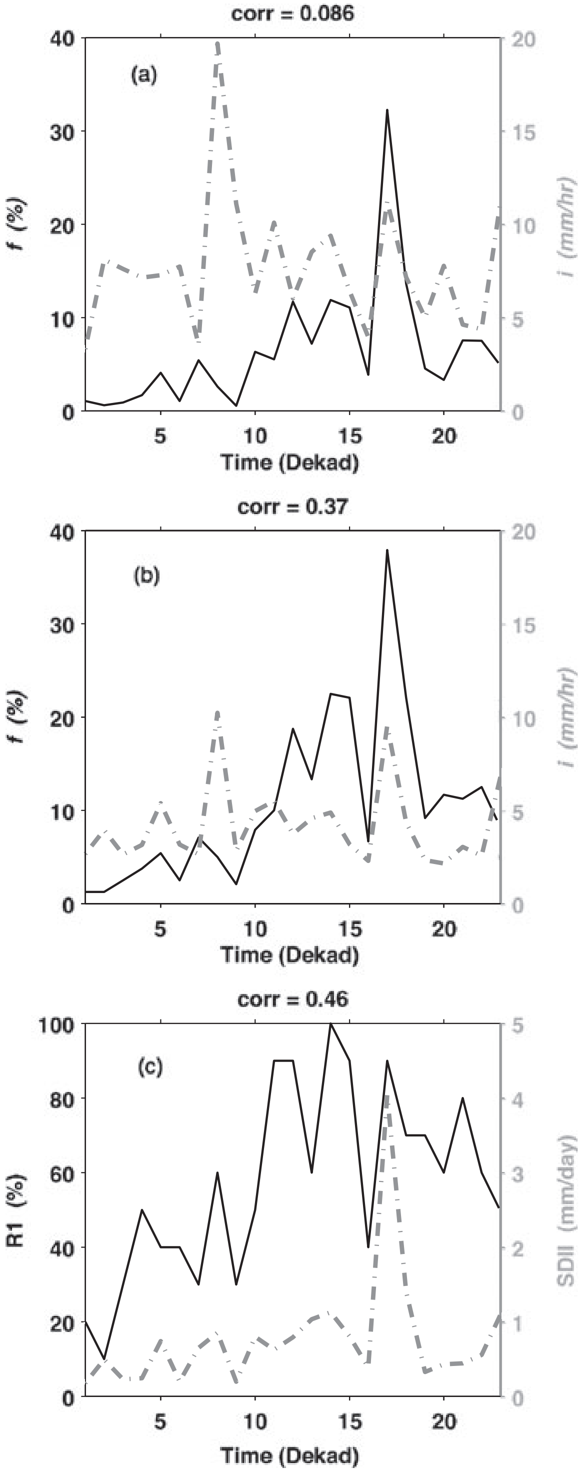

Figure 3. Dekadal mean frequency (black solid line, in %) and intensity (grey, dash-dotted line, in mm h^{-1} in Figures 3a and 3b and mm/day in Figure 3c) of rainfall calculated from rain gauge data at Darwin, Australia. (a) Minute-by-minute rainfall data (a rain event is detected for rain rates >0.4 mm h^{-1}). (b) Hourly-mean data (a rain event is detected for rain rates>0.4 mm h^{-1}). (c) Daily data (a rain event is detected for accumulation >1 mm/day). Dekads are counted starting from September 2010. The correlation between the frequency and intensity time series is noted in the title of each panel.

measurements of daily rainfall. In the following section, we will extend our analysis of *f* and *i* to other areas.

[21] In Figure 4, we show the Hovmoeller diagram of rainfall frequency and intensity averaged over land points over the longitudes 78°E to 83°E (see Figure 1). Figures 4a and 4d are for *f* and *i*, respectively, derived from the TRMM PR data; the Figures 4b and 4e and Figures 4c and 4f are for R1 and SDII derived from daily data from TRMM 3B42 and from the gridded product of the Indian Meteorological Department (IMD), respectively. The inception of the monsoon is characterized by an increase in frequency of rain events and frequency of rainy days (i.e., both *f* and R1) that occur at the same time for all latitudes considered here (10°N to 26°N). The mean daily intensity also goes up during the monsoon season in both TRMM 3B42 and IMD (Figures 4b, 4c): It is at a minimum in May and at a maximum in July and August. After that, it decays slowly: October values are still larger than May values. There are differences between the satellite-based and the ground-based data sets, such as the strength of the maximum of both R1 and SDII in the northern part of the domain, but these differences do not detract from this consistent picture. The PR data (Figure 4a) tell a different story: Conditional intensity (*i*) is at a maximum well before the onset of monsoon season, and it is actually at a relative minimum at the core of the rainy season. During the retreat of the monsoon in October, the PR data show average intensities comparable to those at the onset in June but lower than the spring values. To make the comparison with the daily-based data more straightforward, we have contoured rainfall intensity in mm h^{-1} on top of the dBZ field. The close correspondence of the two measures of intensity indicates that they are interchangeable for our purposes.

[22] We can look further into this data and contrast the joint probability density functions (JPDFs) of frequency and intensity during the core monsoon months and in the prior season (Figure 5). When we use PR data (Figure 5a, 5b), each grid point provides one entry in the distribution for each season, meaning that climatological May–June average *f* and *i* at each grid point in central India contribute to the JPDF of the pre-onset season and climatological July–August–September averages enter the monsoon season JPDF. The region chosen (17°N to 25°N, 78°E to 83°E) has no defined gradients in either frequency or intensity, and therefore the JPDFs describe general characteristics of the area. We compare the JPDFs obtained from TRMM PR data with two definitions of intensity (one using reflectivity and one using rain rates) to the JPDFs obtained from the daily TRMM 3B42 data. In this case, each data point comes from a different grid point and a different year.

[23] There is a substantial overlap between the two seasonal distributions, especially in the PR case, in part due to the fact that we chose May–June as representative of pre-onset conditions even though the Indian monsoon often starts in the middle of June. However, it is clear that the monsoon season is characterized by higher rain frequency (*f*) and more rainy days (R1). Moreover, the PR data indicate that the premonsoon season has a higher mean value of conditional intensity than the monsoon season. This finding is true for all frequencies at which both distributions exist and should therefore be considered a robust, although small, difference. The PR data also show a wider JPDF during May–June,

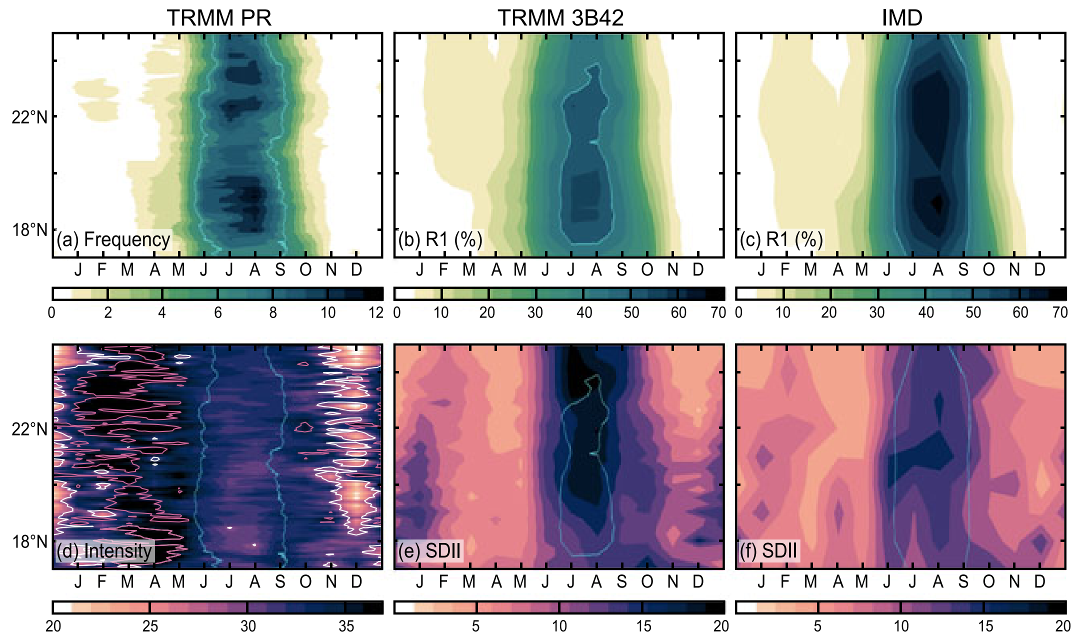

Figure 4. (a) Frequency and (d) intensity of rainfall in the TRMM PR data, (b, e) TRMM 3B42 data, and (c, f) Indian Meteorological Department gridded station data, as a function of latitude and climatological month, averaged over the longitudes of central India (78°E to 83°E). In Figures 4a and 4d, frequency and intensity (f and i) calculated from snapshot values are plotted in units of % and dBZ, respectively. In Figures 4b, 4e and 4c, 4f, frequency and intensity (R1 and SDII) are plotted in units of % and mm/day, respectively. The blue contour is 7% f for instantaneous data and 50% R1 for daily data. The pink and white contours in Figure 4d are representative isolines of rainfall intensity in mm hr^{-1}.

which indicates that mean conditional intensity varies more widely across grid points in the premonsoon season. Conversely, the daily data depict the transition from premonsoon to monsoon as a simple shift of the JPDF toward both higher frequency and higher intensity, which is consistent with Figure 4. We also note that in the PR data set, average summer values of conditional intensity are nearly independent of frequency—except at very low frequency (above about 7% frequency, the mean intensity values are close to constant for all frequencies). As noted in the introduction, contrasting patterns of frequency and intensity could suggest that higher intensity and smaller frequencies are related. However, a negative relationship is inconsistent with the summer JPDF for India (or other locations, as will be explained in the next section). The spring JPDF indicates the opposite behavior: grid points that experience more frequent rainfall also show more intense rainfall, on average. This finding indicates that explanations for the spatial patterns of f and i will have to be

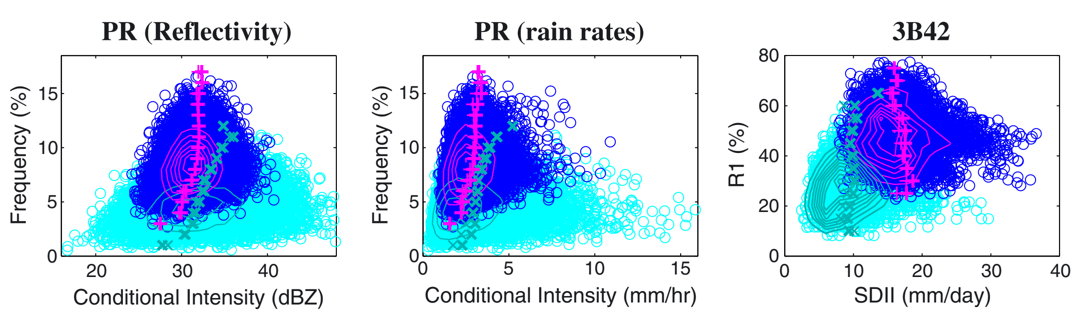

Figure 5. Intensity/Frequency scatterplot (dots), intensity/frequency joint probability density function (contours), and mean and median intensity as a function of frequency (thick and thin symbols, respectively) for May–June (light blue) and July–August–September (dark blue and magenta) averages for central India. TRMM PR data and considering intensity in units of (left) reflectivity (dBZ) and (middle) rain rates (mm hr^{-1}). (right) Daily TRMM 3B42 data, and intensity is in units of mm/day. Data are taken from the central India box. For most frequency values, the mean and median intensity are indistinguishable, supporting the notion that the intensity distributions are close to Gaussian and that discussing them in terms of mean and variance is appropriate. Differences in the pre-onset and rainy-season mean intensity are significant (95% level) at all frequency values, as determined by Monte Carlo testing.

specific to place and time and cannot rely on a general relationship between the two quantities. (Analysis of the whole tropical band supports these conclusions; not shown.)

[24] To understand more thoroughly why the premonsoon season has a wider range of intensities and a higher overall mean intensity, we take advantage of a different data set produced from the TRMM PR: the precipitation feature data set of *Nesbitt et al.* [2000] and *Liu et al.* [2008]. For all rainfall events, this data set provides, among many other parameters, a distinction between convective and stratiform rain amounts and areas [*Houze*, 1993; *Steiner et al.*, 1995; *Awaka et al.*, 1997]. We selected all the events happening in the central India region for the same 10 years on which our climatology is based and compared the relative importance of stratiform and convective rainfall during May–June and July–August. This analysis is summarized in Figure 6. Figures 6a and 6b contrast the month-to-month evolution of accumulated rainfall area and rainfall amounts for both convective and stratiform rainfall. The total pixel counts represent an estimate, based on 10 years of sampling by TRMM, of the sum of the raining area over all the storms during each month (Figure 6a). The total volume of rain (accumulation times area) in the convective and stratiform categories (Figure 6b) is the pixel count weighted by the TRMM estimated near-surface rain rate for each pixel. A comparison between Figures 6a and 6b shows that there is more rain area and rainfall in July–August (monsoon) than in May–June (premonsoon) in both convective and stratiform precipitation categories. The remaining panels in the figure illustrate the monthly variations in the components of total rain area and total rain volume–the average area of a storm in terms of pixel counts (Figure 6c), the storm average volume of rainfall (Figure 6d), the mean rainfall intensities (Figure 6e), and ratio between convective and stratiform rain rates (mean convective ratio) and convective and stratiform areas (Figure 6f). Not shown is the number of precipitation features per month.

[25] The seasonal evolution of rainfall frequency can be traced as the seasonal evolution of total stratiform area (Figure 6a). Whereas the monthly total stratiform area rises from March through July (Figure 6a), the mean size of stratiform precipitation area for each storm increases about 3 times from May to June and then decreases slightly over the next few months (Figure 6c). Hence, both an increased number of storms and increased size of stratiform area within each storm are contributing factors to increasing total stratiform area (Figure 6a). The decreasing ratio of convective to stratiform area between May and July paints the same picture (Figure 6f). Larger stratiform areas are commonly associated with larger MCS with longer durations [*Houze*, 2004]. Total convective area increases from March through July as well (Figure 6a), but the trend in average convective area per storm decreases from May to July and then increases slightly. For convective areas, the larger monthly totals in Figure 6a are more closely related to more storms per month than changes in the convective area per storm.

[26] The stronger conditional intensity during pre-onset months compared to monsoon months can be explained in terms of the balance between stratiform and convective rain area per storm (Figures 6c, 6d, 6f). Storms during pre-onset months have less area experiencing stratiform rain and more area experiencing convective rain (April–May ratio of convective stratiform area of 0.7) than storms during monsoon months (June–July ratio of convective to stratiform area is $\sim$0.2) (Figure 6f). Thus, spring conditional intensities are higher because the low-intensity stratiform rain is less likely to factor into the averaging. Note that when we look at rainfall rates per pixel (Figure 6e), the intensity of convective rain is similar in the pre-onset months and core rainy-season months, whereas the intensity of stratiform rain actually increases slightly from June to September. The higher values of conditional intensity seen in Figure 5 during spring result from the lack of stratiform rain in the samples and not from more explosive convective cells. Similarly, the higher ratio of convective to stratiform rainfall explains the higher variability in conditional intensity in spring because stratiform rain spans a much narrower range of possible intensities than convective rain does [*Steiner et al.*, 1995] and (Figure 6e).

4. The Relationship Between Frequency and Intensity of Rainfall Over Tropical Regions

[27] The purpose of this section is to show that in all tropical land regions, the months before the core rainy season are characterized by a relative prominence of convective rainfall and thus by conditional intensities that are spatially more variable and higher in the mean. First, we survey land regions with seasonal cycles that are fundamentally different from that of India, and then we repeat our analysis on oceanic regions to draw the contrast between continental and maritime environments.

4.1. Other Monsoon Regions

[28] We first focus on two monsoon regions (West Africa and Australia) that differ from India because of their proximity to deserts and the presence of a more complex circulation with a shallow thermal cell superimposed on the deep monsoonal circulation [*Nie et al.*, 2010]. Similar analysis for the monsoon regions of South America and South Africa (Figure 1) produces the same main result of maximum intensity during the pre-onset months. Figure 7 shows the seasonal evolution of rainfall frequency and rainfall intensity averaged over the longitudes of West Africa (5°W to 5°E) and central Australia (130°E to 135°E). In both places, we clearly see the seasonal migration of rainfall, which expands from the ocean to land during the summer season. As before, we see that the rainy season is characterized by more frequent rainfall events. In addition, the onset of the rainy season over land is preceded by a maximum in conditional intensity. This is especially apparent for the Australian region. The land portion of the domain (south of 12°S) sees maximum intensities during October–November–December. In contrast, the ocean region immediately to the north sees a smooth transition between the low values of the dry season to a very broad maximum extending from October to July.

[29] The thick line superimposed on the frequency and intensity fields is the confluence line, the contour of zero meridional wind at the surface. It has long been noted (see, for example, the reference to colonial scientists in Africa in the early 20th century in *Hastenrath* [1991]) that the rain band in these monsoon areas is distinct from the ITCZ. The ITCZ is defined by surface convergence and is closely

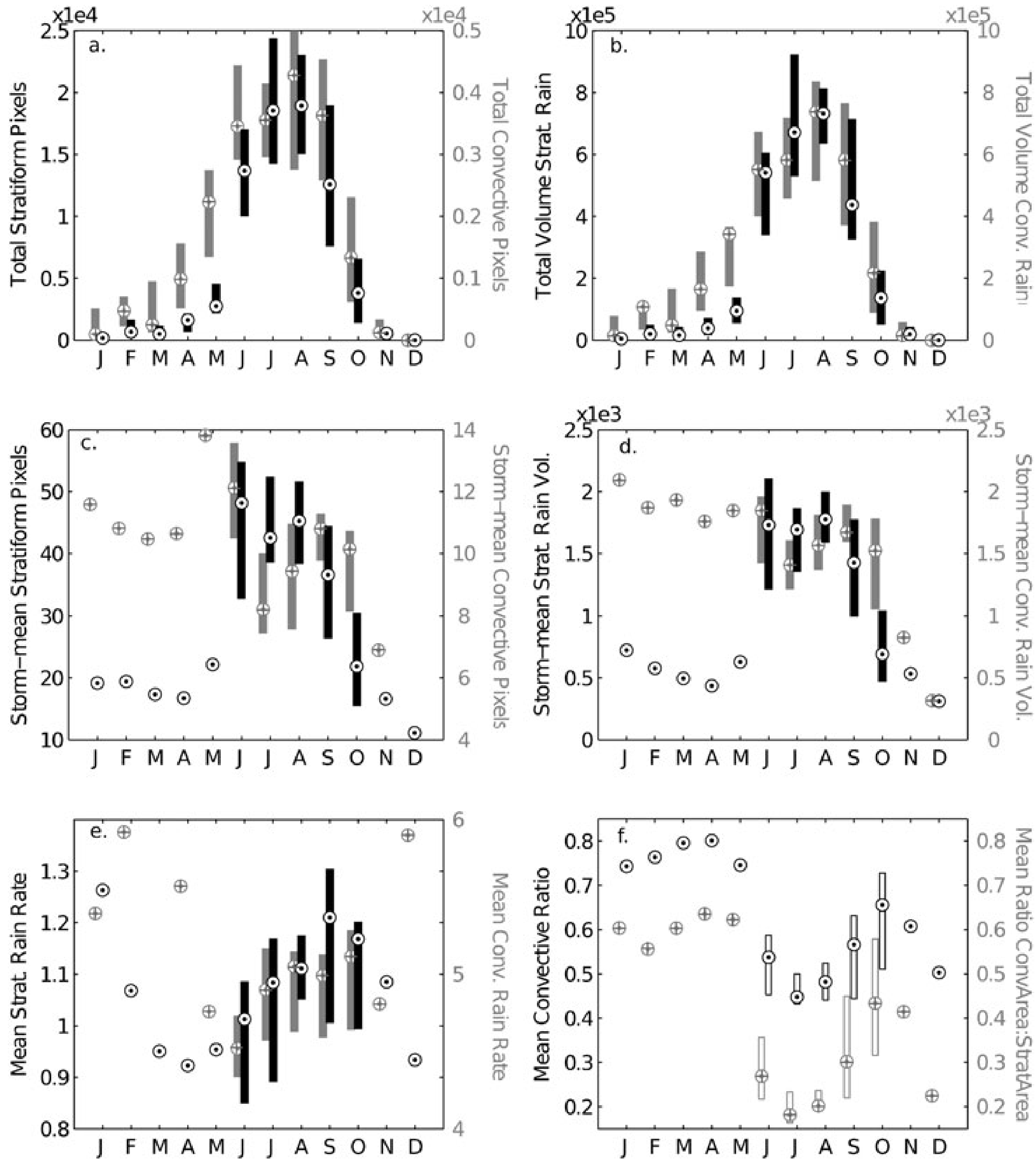

Figure 6. (a–f) Seasonal evolution of stratiform and convective rain for 1998–2007 over central India. For each variable, we plot the 25th and 75th percentile (bar) and the median values (dots) of the 12 individual monthly values. For calendar months with few rain events, only the median is plotted. Area is number of pixels. Rain is volumetric rain. Total refers to the accumulated total for the month. Storm mean is the average across the storms that happened in any given month. Mean rain per pixel is calculated as rain per storm divided by area of the storm, averaged over all the storms occurring in any given month.

related to the meridional confluence line [see also *Nicholson*, 2009]. In the mean, the confluence line marks the surface separation between the moist monsoon wind that flows from the equatorial region and the dry wind that flows from the desert region on the poleward flank; it represents the edge of a shallow direct circulation that flows near the surface from the ocean toward the heat low over the desert, with a return flow above the boundary layer (in West Africa, the return flow is at about 700 mb during the onset season and 500 mb at the peak of the monsoon [*Zhang et al.*, 2006]). The deep convection that makes up the rain band is found equatorward of the confluence line, where the monsoon flow is deeper and convection is not strongly capped by the penetration of the desert air. However, the correspondence between the confluence line and a sharp gradient in conditional intensity over land indicates that the mean picture misses some subtleties: Albeit rarely, deep convection sometimes occurs as far poleward as the monsoon flow can reach—but no

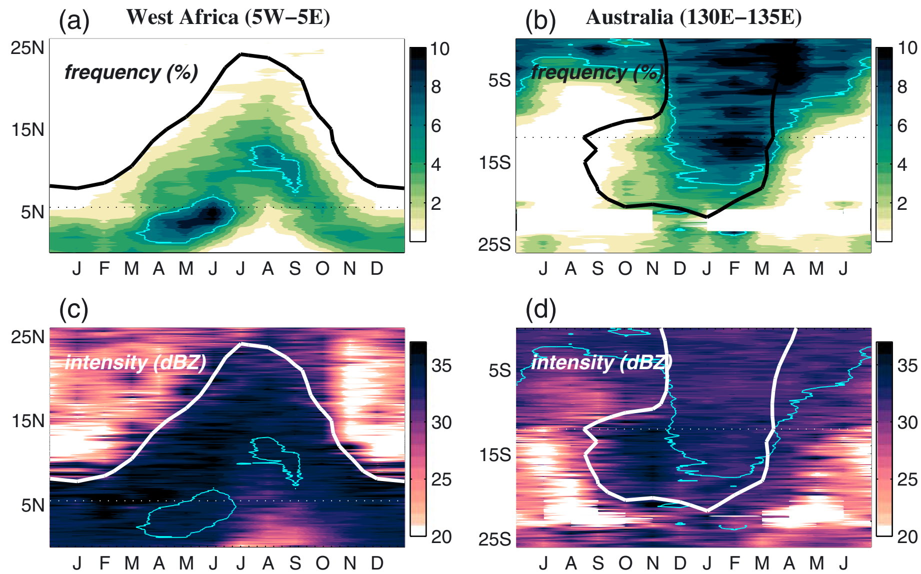

Figure 7. As in Figure 4, left, but for (left) West Africa and (right) Australia. The thick black or white contour is the climatological surface confluence line (i.e., the line of vanishing meridional wind). Note that the calendar is shifted for Australia so that the plot is centered on the rainy season. The approximate boundary between land and ocean is denoted by the dotted lines.

further. In Figure 7, the mean confluence line is located at the approximate boundary for deep convection in both West Africa and Australia. In Australia, the effect is most visible in the pre-onset months and becomes less visible as the monsoon retreats. This difference could be due to the fact that the Australian monsoon is not captured as well by a simple meridional circulation. Alternatively, we speculate that it might be indicative of a real difference in the effectiveness of dry advection in capping deep convection at the beginning of the season, when the land is dry, compared with the end of the season, when the land is moist.

[30] Figures 8 and 9 provide a more quantitative assessment of the difference in conditional intensity between the pre-onset and rainy-season months. The JPDFs of frequency and intensity confirm that the pre-onset months in both regions have mostly higher mean values of conditional intensity and more spatial variability, which is similar to central India (albeit, the differences are smaller). For very low values of frequency of rainfall, mean intensity is actually weaker in the pre-onset months. We interpret this result as a consequence of including in our analysis dry regions at the margin of the monsoon (note that frequencies as low as 3%

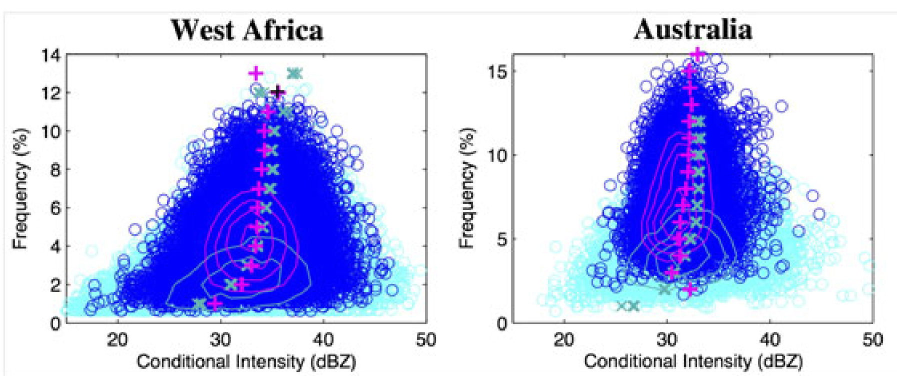

Figure 8. Intensity/Frequency scatterplot (dots), intensity/frequency joint probability density function (contours), and mean and median intensity as a function of frequency (thick and thin symbols, respectively) for pre-onset (light blue) and rainy-season (dark blue and magenta) averages for (left) West Africa and (right) Australia. Pre-onset (rainy season) months are May–June (July–August–September) for West Africa and Nov–Dec (Jan–Feb–Mar) for Australia. Intensity is in units of reflectivity (dBZ). For most frequency values, the mean and median intensity are indistinguishable, supporting the notion that the intensity distributions are close to Gaussian and that discussing them in terms of mean and variance is appropriate. Differences in the pre-onset and rainy-season mean intensity are significant (95% level) at most frequency values, as determined by Monte Carlo testing; seasonal differences are not significant in West Africa for pixels with rain frequency of 12% and this is indicated by a black cross.

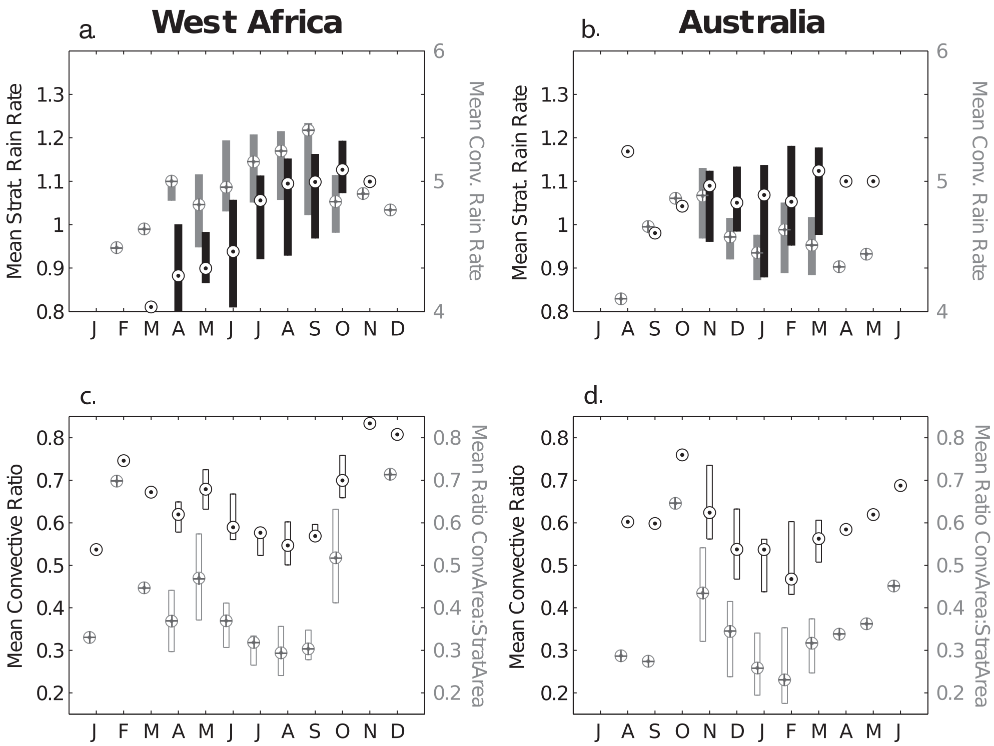

Figure 9. As in Figures 6e, 6f, but for (left) West Africa and (right) Australia. Note that the calendar is shifted for Australia so that the plot is centered on the rainy season.

included in this analysis are absent in central India during the rainy season, Figure 5). The analysis of the precipitation features summarized in Figure 9 confirms that, as seen over India, the core of the rainy season is characterized by events that have smaller convective area and larger stratiform area. The area of convective rainfall relative to that of stratiform rainfall is reduced from pre-onset months to core rainy season by a factor of nearly 2 and 3 in West Africa and Australia, respectively. The rainfall rates per pixel behave differently in different regions. They tend to become higher as the season progresses in Africa, but they are highest in the pre-onset months in Australia. The fact that convective rainfall rates per pixel do not exhibit a consistent seasonal evolution across the monsoon regions, but conditional intensity does, supports the idea that the main reason for higher conditional intensities during the pre-onset months is the prevalent sampling of convective rainfall.

[31] In monsoon regions, the retreat of the rains defines a season comparable to the onset season, but we do not observe a comparable peak in conditional intensity. The asymmetry is especially apparent in Australia, but the reason is unclear.

4.2. Equatorial Land Regions

[32] We complete our survey of tropical land regions by examining South America and central Africa. Our focus is on the equatorial portion of the regions, where some amount of rainfall is present year round.

[33] Figure 10 shows the seasonal evolution of rainfall frequency and intensity. There are notable differences in the annual cycle of rainfall in the two regions: Rainfall frequency over the equatorial Congo has a strong semiannual component, whereas the equatorial Amazon has one strong annual peak in March–April–May. The Congo presents the same relationship between frequency and intensity seen in monsoon regions: peak intensity precedes peak frequency. In South America, we clearly see a maximum in intensity values from August to October when frequency is minimum and consistent with the other regions. However, the region north of the Equator does not behave as expected. During December–January–February, both frequency and intensity experience a relative minimum. As shown below, this behavior is typical of ocean regions. The analysis of the precipitation features (Figure 11) reveals that the intensity peak is due to a maximum in convective area in the Amazon where the relative area of convective to stratiform goes from 0.2 to 0.6 between April and September. This maximum in convective area also occurs in the Congo during June–July–August. The fraction of convective area in the Congo is 0.5 in July and approximately 0.3 in March and October. The January–February–March peak in the Congo is due in part to larger convective areas but mostly due to higher convective intensities.

4.3. Oceanic Regions

[34] Frequency and conditional intensity over oceanic regions follow a different pattern than what is observed over continental regions. Here we present two examples: (1) the central Pacific at the eastern edge of the warm pool, where the ITCZ and the SPCZ merge and rainfall is widespread in the whole domain and (2) the eastern Pacific, where rainfall is dominated by a well-defined ITCZ north of the Equator and a secondary rainfall maximum south of the Equator during boreal spring. The Hovmoeller diagrams of rainfall frequency and intensity are presented in Figure 12. As we would expect from climatological rain rates, rainfall

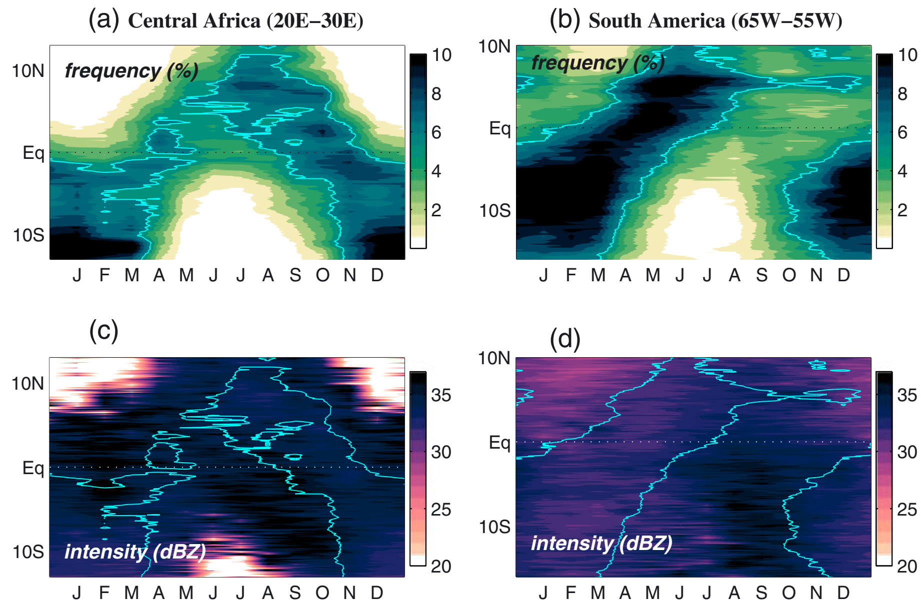

Figure 10. As in Figures 4a, 4d, but for (left) Congo and (right) Amazon.

frequency presents a very sharp maximum in the ITCZ in the eastern Pacific and is more uniform in the central Pacific. Over these oceanic regions, variations in intensity mimic frequency to a large degree. This finding, which is very apparent in the ITCZ of the eastern Pacific, is less apparent in the central Pacific, where the patterns of frequency and intensity are not sharply defined. Unlike continental regions, there is no indication that intensity is higher outside the area of maximum frequency in either the eastern or the central Pacific (or the Atlantic ITCZ; not shown). This implies that the intensity pattern is similar at daily and individual storm timescales. The overall homogeneity of rainfall intensity is confirmed by Figure 13, which shows seasonal variations in storm convective and stratiform area and rain rates. The fraction of convective area relative to stratiform area is minimum when frequency is maximum, as expected, but the seasonal range is trivial in both regions, with the ratio going from 0.15 to 0.25 in the eastern Pacific and staying around 0.25 in the central Pacific (Figure 13d). The seasonal changes in convective rain rates parallel those of

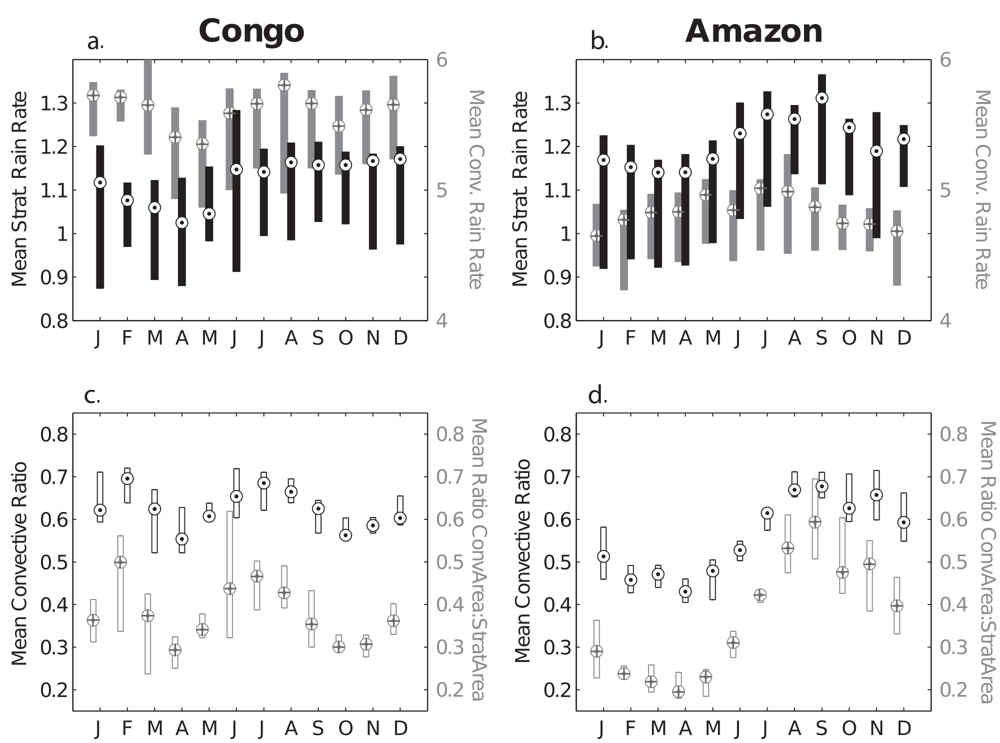

Figure 11. As in Figure 6e, 6f, but for (left) Congo and (right) Amazon.

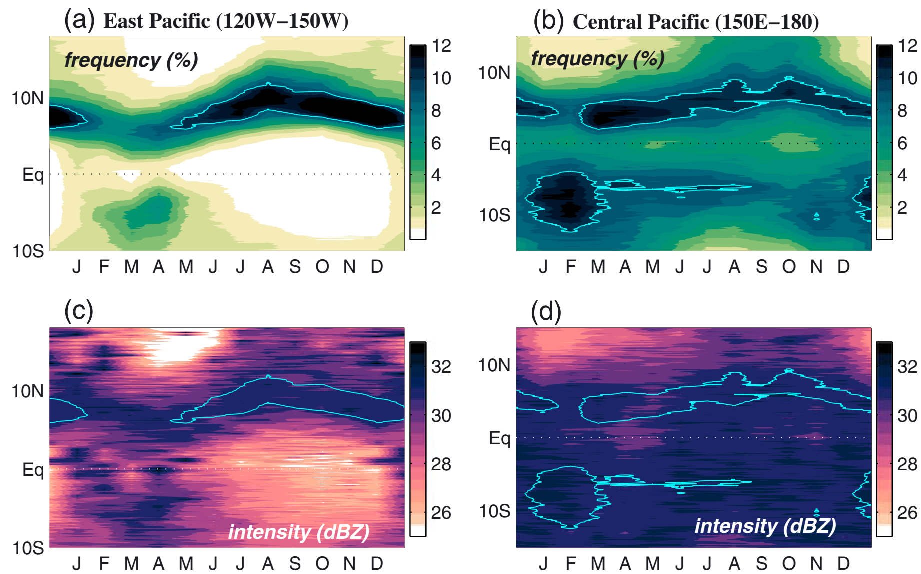

Figure 12. As in Figure 4a, 4d, but for (left) eastern Pacific and (right) central Pacific.

frequency (see, for example, the maximum in the eastern Pacific during northern fall, Figure 13a). The observation that the precipitation structure of individual rainfall events does not change much seasonally over the ocean is also illustrated by the small seasonal variations in ratio of convective area to stratiform area over ocean (Figure 13) as compared to land (Figures 6, 9, and 11).

4.4. Tropic-Wide Comparison

[35] The differences in the seasonal evolution of mean intensity between ocean and land areas—detailed above for selected regions—are robust across the tropical and subtropical band as a whole. This is shown in Figure 14, which composites the seasonal evolution of mean and standard deviation of rain intensity across the rainy season in oceanic and land regions. For each location, *Mo* identifies the month of maximum rainfall frequency and frequency and intensity are plotted for the 7 months centered on the peak month (*Mo* – 3 to *Mo* + 3), averaged over all ocean points, all land points, and land or ocean points with significant rainfall (where peak frequency is above 6%, see *Biasutti et al.* [2011]). Also plotted is the standard deviation across all the grid points in each regional grouping, as a measure of the variability in intensity within each month.

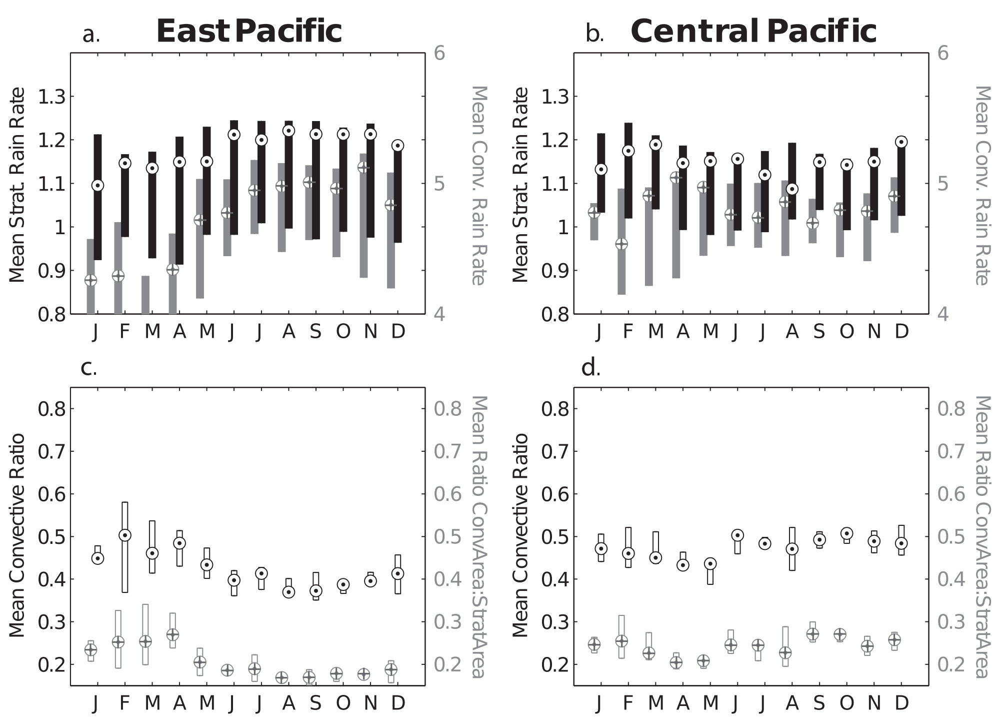

Figure 13. As in Figure 6e, 6f, but for (left) eastern Pacific and (right) central Pacific.

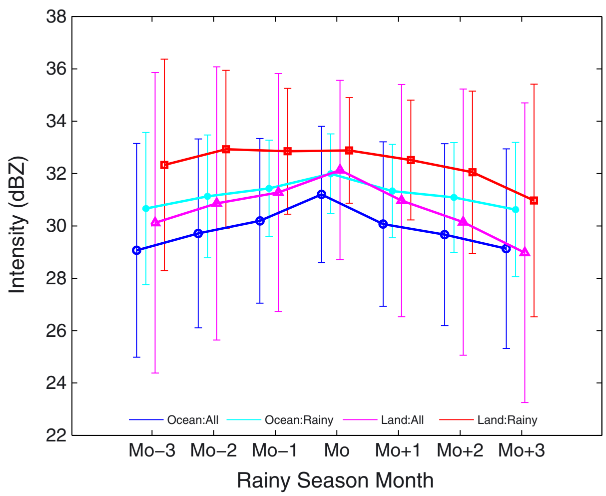

Figure 14. The seasonal evolution of the mean and the variability of rain intensity leading in and out of the rainy season in terms of changes in mean rain intensity (dBZ) for all regions covered by the TRMM PR dataset (±35° latitude). The tropical band is separated into ocean (Ocean:All, blue open dots), land (Land:All, magenta triangle), oceanic regions with maximum monthly-mean rainfall frequency above 6% (Ocean:Rainy, cyan filled dots), and land regions with maximum monthly-mean rainfall frequency above 6% (Land:Rainy, red squares). The error bars represent the standard deviation of monthly mean intensity within the set of grid points associated with each region and time period. The central month (*Mo*) indicates the month of maximum rain frequency determined independently at each grid point. Frequency and intensity values were regridded to 0.5° resolution prior to computing the composite. Abscissas for the four regions are offset for readability.

The analysis confirms our previous claims. The timing of peak frequency and peak intensity coincide over the oceans. Over land, excluding marginal areas of very sporadic convection, the rainy season is preceded (but not followed) by a season of more intense rainfall. In all regions, rain intensity is the least variable when rain frequency is at its peak.

5. Can Aggregated Rainfall Data Characterize Rain Events?

[36] The above analysis has shown that we can learn a great deal about the nature of storms from instantaneous rainfall data: (1) Ocean regions have more frequent and less intense storms than land regions, with little seasonality or spatial gradients in the characteristics of the storms; (2) land regions have considerable variations in storm intensity seasonally and especially spatially (contrast, for example, the Congo and the Amazon or the southwest and southeast United States); and (3) mean rainfall rates in any given land region are more intense during the development than during the core of the rainy season. We now examine if the kind of aggregated rainfall data that is typically output from climate models is sufficient to characterize what kind of storms occur in any given region in any given season.

[37] Previous sections have shown that the preponderance of stratiform or convective rainfall can explain the contrast in rainfall characteristics between land and ocean, as well as seasonal variations over a selected region. Climate models do not explicitly simulate convection, but they do parameterize it, and they distinguish between convective and stratiform (or large-scale) precipitation. Although climate simulations do not output instantaneous values of precipitation, they often do output accumulation of convective and stratiform components at daily and longer timescales. We can, therefore, investigate whether daily values of convective and stratiform precipitation can properly describe storm characteristics across regions and seasons. Our goal is not to assess model biases in the kind of rain events produced but instead to identify if such biases can be detected. Thus, we continue to look at observations, but aggregated in a way comparable to what is available for climate models.

[38] Figure 15 shows the annual mean ratio of convective to stratiform rainfall calculated from TRMM L3 (Level 3 products of the University of Utah Precipitation Measuring Mission data set) and from ERA-Interim reanalysis. In the

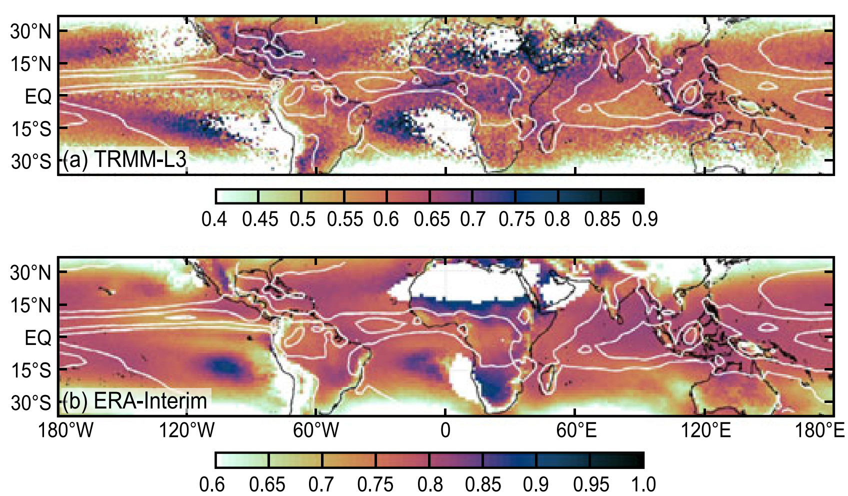

Figure 15. Convective ratio (convective rain to total rain), calculated from (a) TRMM monthly total convective and stratiform rainfall accumulation and (b) ERA-Interim reanalysis daily average convective and stratiform rainfall accumulations.

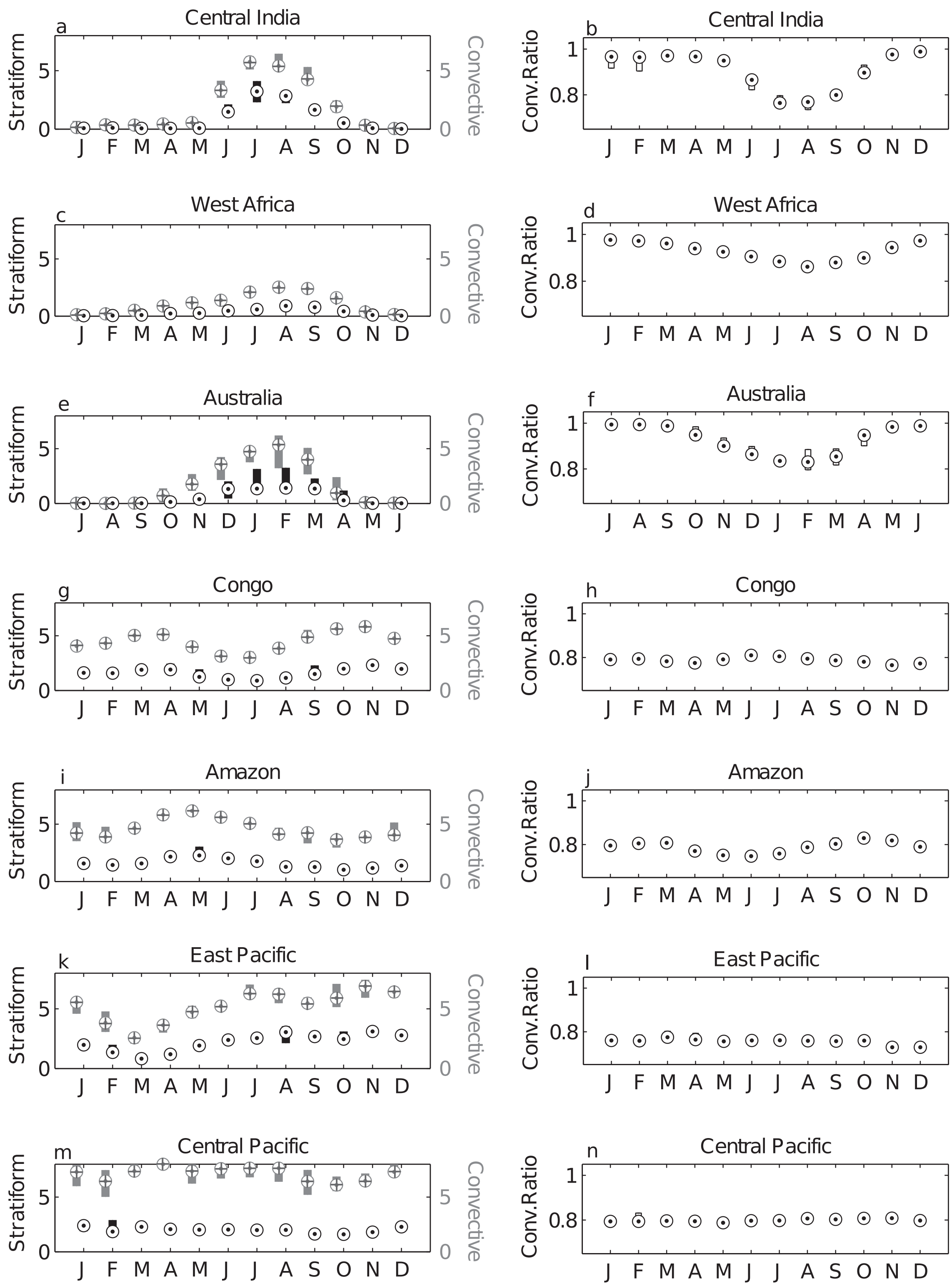

Figure 16. Monthly (left) mean convective and stratiform rainfall and (right) convective ratio from daily values in the ERA-Interim reanalysis for different regions. See titles in each panel and Figure1 for specific regions.

case of TRMM L3, the ratio is calculated from monthly total convective and stratiform rainfall data and then averaged over 120 months (1998–2007). Months with minimal rainfall are masked out so the stratus decks and desert regions appear as missing data. (Note that TRMM does not detect drizzle in stratocumulus.) In the case of the reanalysis, the daily values of convective and stratiform rain are used to calculate the daily ratio, which is then averaged over the same 10 years. ERA-Interim rainfall rates are model output, but they are constrained by the assimilation of radiances [*Dee et al.*, 2011]. There are large differences across the two estimates that are probably due to model bias combined with measurement deficiencies and averaging choices. These differences are beyond the scope of our discussion. (The performance of the reanalysis is addressed in *Dee et al.* [2011]). What interests us is that both estimates capture some features of the instantaneous intensity pattern shown in Figure 2b but not its overall pattern. For example, local maxima in the Himalayan Indentation and in the Sahel are captured by both the convective ratio, as calculated from these aggregated rainfall data, and the intensity. (The regions of high convective ratio at the margin of the stratus decks are artifacts following from the division of two small numbers.) However, the convective ratio does not adequately capture the broad difference in intensity between land and ocean or between the ITCZ regions and oceanic regions nearby, and it does not adequately capture the extreme intensities in the Congo and the American Plains. If we consider the TRMM data, we can ascribe the discrepancies between instantaneous intensity (Figure 2b) and monthly convective fraction (Figure 15a) to the fact that rainfall data have been aggregated in time. This assertion is proved by comparing our estimates of convective ratio to the estimate provided by *Schumacher and Houze* [2003], which was calculated from instantaneous data and which clearly highlights high convective ratios in those regions where we see high instantaneous intensity. (Note that Figure 3 in *Schumacher and Houze* [2003] shows stratiform ratio, which is the complement to convective ratio. Thus, a minimum in one is a maximum in the other.)

[39] Despite its previously discussed limitations, the aggregated convective ratio can still convey useful information about the spatial distribution of and seasonal changes in storm intensity. To show this, we present regional averages of convective and stratiform daily rainfall estimated from ERA-Interim (Figure 16). As mentioned before, both daily convective and stratiform rainfall rates are highest at the peak of the rainy season because daily rain rates integrate values of instantaneous rain rates and rain frequency. At the same time, the daily convective ratio matches instantaneous observations in two important ways: (1) It declines during the core of the rainy seasons in each region, and (2) it shows a seasonal range that is largest in monsoon regions, reduced over other continental lands, and negligible over the oceans. These distinctions suggest that this measure of convective ratio captures—at least qualitatively—some of the spatial differences and seasonality of storm characteristics.

[40] We conclude that the ratio of convective to stratiform rainfall, even when aggregated at daily timescales, is useful to monitor the seasonal changes in storm intensity in a variety of environments. However, it is not sufficient to distinguish the mean storm intensity in different regions. To do so, it is necessary to consider conditional intensity at much higher temporal resolution.

6. Summary and Conclusion

[41] The need for a better description of the range and controls of rainfall intensity at hourly or shorter timescales is acute. This is particularly true for the tropics, where some very intense storms occur and the infrastructure of cities and agriculture alike is extremely vulnerable.

[42] The TRMM PR has taken snapshots of the three-dimensional structure of rainfall events since 1998, providing a unique insight into the nature of tropical rainfall. We use two data sets derived from this instrument to assess the seasonal variations of rainfall intensity at the scale of individual rain events and to determine the associated variations in storm structure. The first data set [*Biasutti et al.*, 2011] is a gridded monthly climatology of the frequency and conditional intensity of rainfall events. The second data set [*Liu et al.*, 2008] is organized by storm and is used in this work to determine the relative contribution of stratiform to convective rainfall in each event.

[43] On average, the highest rainfall intensities occur over land and have a distinct seasonality. Over most tropical land, peak rainfall accumulation does not occur at the same time as peak rainfall intensity. Instead, the months preceding the core of the rainy season, when frequency of rainfall is still low, show the highest conditional intensity. This high intensity is due to a high prevalence of convective precipitation areas and fewer developed stratiform precipitation areas. The total convective area increases during the rainy season; however, stratiform areas grow more and become dominant, so the average rainfall intensity declines as frequency of rainfall increases. While previous studies have addressed these points regionally (see, for example, [*Zipser et al.*, 2006] and further examples discussed in section 1), we present a tropic-wide systematic survey and show that variations in precipitation structures between the development phase and the core of the rainy season are nearly consistent in different geographic regions (i.e., in the monsoon regions of India, West Africa, Australia, South America, South Africa, and in equatorial land regions). Over the ocean, the highest intensity coincides with highest rain frequency and thus highest rain accumulation. Here, the convective precipitation rain rates are higher at times of more frequent rainfall and variations in the ratio of convective to stratiform area are too small to fully compensate for this effect.

[44] The climate community's work on extreme precipitation in the Tropics has focused primarily on tropical cyclones or on the highest percentiles of daily rainfall accumulation, and has often been limited to oceanic regions. Our observational analysis indicates that these limitations are problematic. First, we have illustrated that daily accumulations are not sufficient to capture the occurrence of individual intense storms because high accumulations can result from a short period of high-intensity rainfall, a higher frequency of lower-intensity rainfall, or some combination of the two. For example, we have shown that neither the SDII nor the convective ratio calculated from daily aggregated data provide any indication of the occurrence of very intense storms over the Congo. The daily timescale is relevant for certain impacts, but it is important to consider that high daily intensity and high storm intensity do not typically coincide. Second, we have shown that seasonal variations in the ratio of stratiform to convective rainfall are large over land and small over ocean. The marked seasonality in storm characteristics over land is in sharp contrast to the relative homogeneity of oceanic storms. Thus, when trying to understand how a changing climate will affect extreme pre-

cipitation, we should be mindful that scalings that are valid over the oceans may not be pertinent to extremes over land.

[45] Finally, we have shown that some aspects of the seasonal variations in precipitation structure over land can be validated with current climate model outputs—namely, the daily convective and stratiform rainfall accumulation. However, to better differentiate storms (for example, between those characteristic of the Congo versus the Amazon), it is necessary to first calculate the instantaneous rainfall intensity and convective rainfall ratio at each model time step and then output their daily averages. Given the importance of understanding how extreme precipitation will change over land regions—including at the timescale of individual storms—we suggest that these quantities also be saved as routine output by climate models.

[46] **Acknowledgments.** ECMWF ERA-Interim data used in this study have been provided by ECMWF (http://data-portal.ecmwf.int/). The precipitation feature data set was obtained from the University of Utah Precipitation Measuring Mission pages (http://trmm.chpc.utah.edu/). The TRMM 3B42 data were obtained from the IRI data library (http://iridl.ldeo.columbia.edu/). The Indian Meteorology Department data were obtained through Erika Coppola of the International Center for Theoretical Physics. Rain gauge data for Darwin was obtained from the ARM Climate Research Facility (http://www.archive.arm.gov/). This work was supported by NASA grant NNX07AD21G and NSF grants ATM-0544766, ATM-0908420, and SES-1048946. Any opinions, findings, and conclusions or recommendations expressed in this material are those of the authors and do not necessarily reflect the views of NASA or NSF.

References

Alexander, L., et al. (2006), Global observed changes in daily climate extremes of temperature and precipitation, *J. Geophys. Res.*, *111*, D05109, doi:10.1029/2005JD006290.

Allen, M. R., and W. J. Ingram (2002), Constraints on future changes in climate and the hydrologic cycle, *Nature*, *419*, 224–232.

Awaka, J., T. Iguchi, H. Kumagai, and K. Okamoto (1997), Rain type classification algorithm for TRMM precipitation radar, in *IGARSS'97. 1997 IEEE International Geoscience and Remote Sensing Symposium Proceedings. Remote Sensing - A Scientific Vision for Sustainable Development*, pp. 1633–1635, IEEE, Singapore.

Biasutti, M., S. E. Yuter, C. D. Burleyson, and A. H. Sobel (2011), Very high resolution rainfall patterns measured by TRMM precipitation radar: Seasonal and diurnal cycles, *Clim. Dyn.*, *39*, 239–258, doi:10.1007/s00382-011-1146-6.

Brooks, H. E., J. W. Lee, and J. P. Craven (2003), The spatial distribution of severe thunderstorm and tornado environments from global reanalysis data, *Atmos. Res.*, *67–68*, 73–94.

Cecil, D. J., S. J. Goodman, D. J. Boccippio, E. J. Zipser, and S. W. Nesbitt (2005), Three years of TRMM precipitation features. Part I: Radar, radiometric, and lightning characteristics, *Mon. Weather Rev.*, *133*, 543–566.

Dai, A. (2001), Global precipitation thunderstorm frequencies. Part I: Seasonal and interannual variations, *J. Clim.*, *14*, 1092.

Dee, D. P., et al. (2011), The ERA-Interim reanalysis: Configuration and performance of the data assimilation system, *Q. J. R. Meteorolog. Soc.*, *137*, 553–597.

Hastenrath, S. (1991), *Climate Dynamics of the Tropics*, Kluwer Academic Publishers-, Dordrecht, The Netherlands.

Hirose, M., and K. Nakamura (2005), Spatial and diurnal variation of precipitation systems over Asia observed by the TRMM precipitation radar, *J. Geophys. Res.*, *110*, D05106, doi:10.1029/2004JD004815.

Houze, R. A. (2004), Mesoscale convective systems, *Rev. Geophys.*, *42*, RG4003, doi:10.1029/2004RG000150.

Houze, R. A. Jr. (1993), *Cloud Dynamics*, Academic Press, San Diego, CA.

Huffman, G., D. Bolvin, E. Nelkin, D. Wolff, R. Adler, G. Gu, Y. Hong, K. Bowman, and E. Stocker (2007), The TRMM Multisatellite Precipitation Analysis (TMPA): Quasi-global, multiyear, combined-sensor precipitation estimates at fine scales, *J. Hydrometeorol.*, *8*, 38–55.

Huffman, G. J., et al. (1997), The global precipitation climatology project (GPCP) combined precipitation data set, *Bull. Amer. Meteor. Soc.*, *78*, 5–20.

Knutson, T. R., et al. (2010), Tropical cyclones and climate change, *Nat. Geosci.*, *3*, 157–163.

Kodama, Y.-M., A. Ohta, M. Katsumata, S. Mori, S. Satoh, and H. Ueda (2005), Seasonal transition of predominant precipitation type and lightning activity over tropical monsoon areas derived from TRMM observations, *Geophys. Res. Lett.*, *32*, L14710, doi:10.1029/2005GL022986.

Kummerow, C., et al. (2000), The status of the Tropical Rainfall Measuring Mission (TRMM) after two years in orbit, *J. Appl. Meteorol.*, *39*, 1965–1982.

Laing, A. G., and J. M. Fritsch (2000), The large-scale environments of the global populations of mesoscale convective complexes, *Mon. Weather Rev.*, *128*, 2756–2776.

Lenderink, G., and E. Van Meijgaard (2008), Increase in hourly precipitation extremes beyond expectations from temperature changes, *Nat. Geosci.*, *1*, 511–514.

Lenderink, G., and E. van Meijgaard (2010), Linking increases in hourly precipitation extremes to atmospheric temperature and moisture changes, *Environ. Res. Lett.*, *5*, 025208.

Lenderink, G., H. Y. Mok, T. C. Lee, and G. J. van Oldenborgh (2011), Scaling and trends of hourly precipitation extremes in two different climate zones—Hong Kong and the Netherlands, *Hydrol. Earth Syst. Sci.*, *15*, 3033–3041.

Liu, C. (2011), Rainfall contributions from precipitation systems with different sizes, convective intensities, and durations over the tropics and subtropics, *J. Hydrometeorol.*, *12*, 394–412.

Liu, C., and E. J. Zipser (2005), Global distribution of convection penetrating the tropical tropopause, *J. Geophys. Res.*, *110*, D23104, doi:10.1029/2005JD006063.

Liu, C., and E. J. Zipser (2008), Diurnal cycles of precipitation, clouds, and lightning in the tropics from 9 years of TRMM observations, *Geophys. Res. Lett.*, *35*, L04819, doi:10.1029/2007GL032437.

Liu, C., and E. J. Zipser (2009), "Warm Rain" in the tropics: Seasonal and regional distributions based on 9 yr of TRMM data, *J. Clim.*, *22*, 767–779.

Liu, C., E. J. Zipser, D. J. Cecil, S. W. Nesbitt, and S. Sherwood (2008), A cloud and precipitation feature Database from nine years of TRMM observations, *J. Appl. Meteorol. Clim.*, *47*, 2712–2728.

Markowski, P., and Y. Richardson (2010), *Mesoscale Meteorology in Midlatitudes, Vol. 2 of Advances in Weather and Climate*, Wiley-Blackwell, Chichester, West Sussex, UK; Hoboken, NJ.

McCollum, J. R., A. Gruber, and M. B. Ba (2000), Discrepancy between gauges and satellite estimates of rainfall in equatorial Africa, *J. Appl. Meteorol.*, *39*, 666–679.

McPhaden, M. J., et al. (1998), The tropical ocean-global atmosphere observing system: A decade of progress, *J. Geophys. Res.*, *103*, 14,169.

Muller, C. J., P. A. O'Gorman, and L. E. Back (2011), Intensification of precipitation extremes with warming in a cloud-resolving model, *J. Clim.*, *24*, 2784–2800.

Negri, A., T. Bell, and L. Xu (2002), Sampling of the diurnal cycle of precipitation using TRMM, *J. Atmos. Oceanic Technol.*, *19*, 1333–1344.

Nesbitt, S., and E. Zipser (2003), The diurnal cycle of rainfall and convective intensity according to three years of TRMM measurements, *J. Clim.*, *16*, 1456–1475.

Nesbitt, S., E. Zipser, and D. Cecil (2000), A census of precipitation features in the Tropics using TRMM: Radar, ice scattering, and lightning observations, *J. Clim.*, *13*, 4087–4106.

Nesbitt, S., E. Zipser, and C. D. Kummerow (2004), An examination of version-5 rainfall estimates from the TRMM microwave imager, precipitation radar, and rain gauges on global, regional, and storm scales, *J. Appl. Meteorol.*, *43*, 1016–1036.

Nesbitt, S. W., R. Cifelli, and S. A. Rutledge (2006), Storm morphology and rainfall characteristics of TRMM precipitation features, *Mon. Weather Rev.*, *134*, 2702–2721.

Nicholson, S. E. (2009), A revised picture of the structure of the "monsoon" and land ITCZ over west Africa, *Clim. Dyn.*, *32*, 1155–1171.

Nie, J., W. R. Boos, and Z. Kuang (2010), Observational evaluation of a convective quasi-equilibrium view of monsoons, *J. Clim.*, *23*, 4416–4428.

O'Gorman, P., and T. Schneider (2009), The physical basis for increases in precipitation extremes in simulations of 21st-century climate change, *P. Natl. A. Sci.*, *106*, 14, 773.

Ramage, C. S. (1971), *Monsoon Metereology*, no. 15 in International Geophysics Series, Academic Press, San Diego, CA.

Romatschke, U., and R. A. Jr. Houze (2010), Extreme summer convection in South America, *J. Clim.*, *23*, 3761–3791.

Romatschke, U., S. Medina, and R. A. Jr. Houze (2010), Regional, seasonal, and diurnal variations of extreme convection in the South Asian region, *J. Clim.*, *23*, 419–439.

Schultz, D. M., and P. N. Schumacher (1999), The use and misuse of conditional symmetric instability, *Mon. Weather. Rev.*, *127*, 2709–2732.

Schumacher, C., and R. A. Houze Jr. (2003), Stratiform rain in the tropics as seen by the TRMM precipitation radar*, *J. Clim.*, *16*, 1739–1756.

Schumacher, C., and R. A. Houze Jr. (2006), Stratiform precipitation production over sub-Saharan Africa and the tropical East Atlantic as observed by TRMM, *Q. J. R. Meteorol. Soc.*, *132*, 2235–2255.
Shaw, S. B., A. A. Royem, and S. J. Riha (2011), The relationship between extreme hourly precipitation and surface temperature in different hydroclimatic regions of the United States, *J. Hydrometeorol.*, *12*, 319–325.
Shige, S., H. Sasaki, K. Okamoto, and T. Iguchi (2006), Validation of rainfall estimates from the 785 TRMM precipitation radar and microwave imager using a radiative transfer model: 1. Comparison of the version-5 and -6 products, *Geophys. Res. Lett.*, *33*, L13803, doi:10.1029/2006GL026350.
Steiner, M., R. A. Houze Jr., and S. E. Yuter (1995), Climatological characterization of three-dimensional storm structure from operational radar and rain gauge data, *J. Appl. Meteorol.*, *34*, 1978–2007.
Tebaldi, C., K. Hayhoe, J. Arblaster, and G. Meehl (2006), Going to the extremes, *Clim. Change*, *79*, 185–211.
Toracinta, E. R., D. Cecil, E. Zipser, and S. Nesbitt (2002), Radar, passive microwave, and lightning characteristics of precipitating systems in the tropics, *Mon. Weather Rev.*, *130*, 802–824.
Trapp, R. J., N. Diffenbaugh, H. E. Brooks, M. E. Baldwin, E. D. Robinson, and J. S. Pal (2007), Changes in severe thunderstorm environment frequency during the 21st century caused by anthropogenically enhanced global radiative forcing, *Proc. Natl. Acad. Sci.*, *104*, 19, 719–19, 723.
Trenberth, K. E., A. Dai, R. M. Rasmussen, and D. B. Parsons (2003), The changing character of precipitation, *Bull. Am. Meteorol. Soc.*, *84*, 1205–1217.
Vecchi, G., and B. Soden (2007), Global warming and the weakening of the tropical circulation, *J. Clim.*, *20*, 4316–4340.
Williams, E., et al. (2002), Contrasting convective regimes over the Amazon: Implications for cloud electrification, *J. Geophys. Res.*, *107*(D20), 8082, doi:10.1029/2001JD000380.
Xie, P., and P. A. Arkin (1997), Global precipitation: A 17-year monthly analysis based on gauge observations, satellite estimates, and numerical model outputs, *Bull. Amer. Meteor. Soc.*, *78*, 2539–2558.
Yuter, S. E., and R. A. Houze (1998), The natural variability of precipitating clouds over the western Pacific warm pool, *Q. J. R. Meteorol. Soc.*, *124*, 53–99.
Zhang, C., P. Woodworth, and G. Gu (2006), The seasonal cycle in the lower troposphere over West Africa from sounding observations., *Q. J. R. Meteorol. Soc.*, *132*, 2561–2584.
Zipser, E., C. Liu, D. Cecil, S. Nesbitt, and D. Yorty (2006), Where are the most intense thunderstorms on Earth? *Bull. Am. Meteorol. Soc.*, *87*, 1057–1071.